





LETTER TO THE EDITOR

Discovery of benzyne, *o*-C₆H₄, in TMC-1 with the QUIJOTE line survey[★]

J. Cernicharo¹, M. Agúndez¹ , R. I. Kaiser², C. Cabezas¹ , B. Tercero^{3,4} , N. Marcelino¹,
J. R. Pardo¹ , and P. de Vicente³

¹ Grupo de Astrofísica Molecular, Instituto de Física Fundamental (IFF-CSIC), C/ Serrano 121, 28006 Madrid, Spain
e-mail: jose.cernicharo@csic.es

² Department of Chemistry, University of Hawaii at Manoa, Honolulu, HI 96822, USA

³ Centro de Desarrollos Tecnológicos, Observatorio de Yebes (IGN), 19141 Yebes, Guadalajara, Spain

⁴ Observatorio Astronómico Nacional (OAN, IGN), Madrid, Spain

Received 28 June 2021 / Accepted 30 July 2021

ABSTRACT

We report the detection, for the first time in space, of a new non-functionalised hydrocarbon cycle in the direction of TMC-1: *o*-C₆H₄ (ortho-benzyne). We derive a column density for this hydrocarbon cycle of $(5.0 \pm 1.0) \times 10^{11} \text{ cm}^{-2}$. The abundance of this species is around 30 times lower than that of cyclopentadiene and indene. We compare the abundance of benzyne with that of other pure hydrocarbons, cycles or chains, and find that it could be formed from neutral-radical reactions such as C₂H + CH₂CHCCH and C + C₅H₅, and possibly through C₄H + C₂H₄, C₃H + CH₂CCH₂, and C₃H₂ + C₃H₃. Hence, the rich content of hydrocarbon cycles observed in TMC-1 could arise through a bottom-up scenario involving reactions of a few radicals with the abundant hydrocarbons recently revealed by the QUIJOTE line survey.

Key words. molecular data – line: identification – ISM: molecules – ISM: individual objects: TMC-1 – astrochemistry

1. Introduction

The recent discovery with the QUIJOTE¹ line survey of abundant hydrocarbons such as the propargyl radical (CH₂CCH), vinylacetylene (CH₂CHCCH), and ethynylallene (H₂CCCHCCH) and cyclic hydrocarbons such as cyclopentadiene (*c*-C₅H₆) and indene (*c*-C₉H₈) in the cold dark cloud TMC-1 (Agúndez et al. 2021a; Cernicharo et al. 2021a,b,c; Burkhardt et al. 2021), as well as the detection of their cyano derivatives (McGuire et al. 2018, 2021) in the same source, points to a new and interesting chemistry that had been completely unforeseen by the most sophisticated state-of-the-art chemical models. The detection of indene, the first non-functionalised polycyclic aromatic hydrocarbons (PAHs) detected in space, in the unexpected environment of a cold starless core is surprising and introduces new challenges to our understanding of the place where these PAHs are formed in space.

Many efforts have been devoted over the last 40 years to understanding the chemical processes that lead to the formation of these molecular species (see e.g. Jones et al. 2011; Parker et al. 2012; Joblin & Cernicharo 2018). Circumstellar envelopes around carbon-rich asymptotic giant branch (AGB) stars have been suggested as the factories of PAHs (Cherchneff et al. 1992). However, PAHs are only detected in well-UV-illuminated regions of the interstellar medium. The detection of benzene in the carbon-rich protoplanetary nebula

CRL 618 (Cernicharo et al. 2001) suggests a bottom-up approach in which the small hydrocarbons that formed during the AGB phase, such as C₂H₂ and C₂H₄, interact with the UV radiation produced by the star in its evolution to the white dwarf phase (Woods et al. 2002; Cernicharo 2004). Other hypotheses involve the processing of dust grains around evolved stars, either through UV photons (Pillari et al. 2015) or by chemical processes (Martínez et al. 2020). Hence, it has been surprising to see that pure PAHs and their cyanide derivatives have been found in TMC-1, which is well protected against UV radiation (Cernicharo et al. 2021c; Burkhardt et al. 2021; McGuire et al. 2018, 2021). It is unlikely that these molecules arise from a reservoir existing since the early stages of the cloud because these relatively small PAHs would not have survived the diffuse cloud stage. An in situ formation mechanism for benzene, cyclopentadiene, indene, and naphthalene must involve abundant hydrocarbons containing from two to five carbon atoms (Kaiser & Hansen 2021). Moreover, some of these species should allow an easy cyclisation in bimolecular reactions to efficiently form the first aromatic ring – benzene (*c*-C₆H₆), benzyne (*c*-C₆H₄), the phenyl radical (*c*-C₆H₅), or any other species – from which larger PAHs can grow (Jones et al. 2011; Parker et al. 2012; McCabe et al. 2020; Doddipatla et al. 2021). The propargyl radical and the closed-shell hydrocarbons methyl-, vinyl-, and ethynylallene have been detected in TMC-1 with high abundances (Agúndez et al. 2021a; Cernicharo et al. 2021b,c). Detecting all possible products of the reactions between these hydrocarbons and radicals is a mandatory step towards understanding the chemistry of PAHs in cold dark clouds.

The name benzyne refers to three isomeric species with molecular formula *c*-C₆H₄, which are six-membered rings with four hydrogen atoms. They can be considered as derivatives

[★] Based on observations carried out with the Yebes 40 m telescope (projects 19A003, 20A014, 20D023, and 21A011). The 40 m radio telescope at Yebes Observatory is operated by the Spanish Geographic Institute (IGN; Ministerio de Transportes, Movilidad y Agenda Urbana).

¹ Q-band Ultrasensitive Inspection Journey to the Obscure TMC-1 Environment.

of benzene molecules due to the loss of two hydrogen atoms. The most stable isomer is 1,2-didehydrobenzene (ortho-benzyne), followed by 1,3-didehydrobenzene (meta-benzyne) and the 1,4-didehydrobenzene (para-benzyne), placed at 147 and 220 kJ mol⁻¹ from the ortho-benzyne, respectively (Olsen 1971). The molecular structure of ortho-benzyne (hereinafter referred to as benzyne or as *o*-C₆H₄) is interesting because it contains a formal triple bond ('-yne') within a six-membered ring (see Fig. 1). This peculiar structure confers a high reactivity, and thus it is a reactive intermediate in organic chemistry that plays an important role in aromatic nucleophilic substitution reactions. In addition, it is a potential key species in the formation of PAHs and soot in pyrolysis experiments of organic molecules (Hirsch et al. 2018).

In this Letter we report the discovery of the ortho isomer of benzyne, *o*-C₆H₄, and we discuss the relative abundances of pure hydrocarbons, chains and cycles, in the context of chemical models that include new radical-neutral reactions involving the abundant hydrocarbons recently found in TMC-1 (Agúndez et al. 2021a; Cernicharo et al. 2021a,b,c). We also discuss the evolution of these molecules when the volume density increases due to the gravitational collapse of the core to form protostars and their dusty planetary disks.

2. Observations

New receivers, built within the Nanocosmos project² and installed at the Yebes 40 m radio telescope, were used for the observations of TMC-1 ($\alpha_{J2000} = 4^{\text{h}}41^{\text{m}}41.9^{\text{s}}$ and $\delta_{J2000} = +25^{\circ}41'27.0''$). A detailed description of the system is given by Tercero et al. (2021). The receiver consists of two cold high electron mobility transistor amplifiers that cover the 31.0–50.3 GHz band with horizontal and vertical polarisations. Receiver temperatures in the runs achieved in 2020 vary from 22 K at 32 GHz to 42 K at 50 GHz. Some power adaptation in the down-conversion chains have reduced the receiver temperatures in 2021 to 16 K at 32 GHz and 25 K at 50 GHz. The back ends are $2 \times 8 \times 2.5$ GHz fast Fourier transform spectrometers with a spectral resolution of 38.15 kHz, providing the whole coverage of the *Q* band in both polarisations. All observations were performed in the frequency switching mode. The main beam efficiency varies from 0.6 at 32 GHz to 0.43 at 50 GHz. The intensity scale used in this work, antenna temperature (T_{A}^*), was calibrated using two absorbers at different temperatures and the atmospheric transmission model ATM (Cernicharo 1985; Pardo et al. 2001). Calibration uncertainties were adopted to be 10%. All data were analysed using the GILDAS package³.

The QUIJOTE line survey was performed in several sessions between 2019 and 2021. Previous QUIJOTE results on the detection of C₃N⁻ and C₅N⁻ (Cernicharo et al. 2020a), HC₅NH⁺ (Marcelino et al. 2020), HC₄NC (Cernicharo et al. 2020b), and HC₃O⁺ (Cernicharo et al. 2020c) were based on two observing runs performed in November 2019 and February 2020. Two different frequency coverages were achieved during these runs, 31.08–49.52 GHz and 31.98–50.42 GHz, in order to check that no spurious spectral ghosts are produced in the down-conversion chain. In these observations the frequency throw was 10 MHz.

Additional data were taken in October 2020, December 2020, and January–May 2021. In these observations the selected frequency coverage was 31.08–49.52 GHz, and the frequency throw for the frequency switching observations was

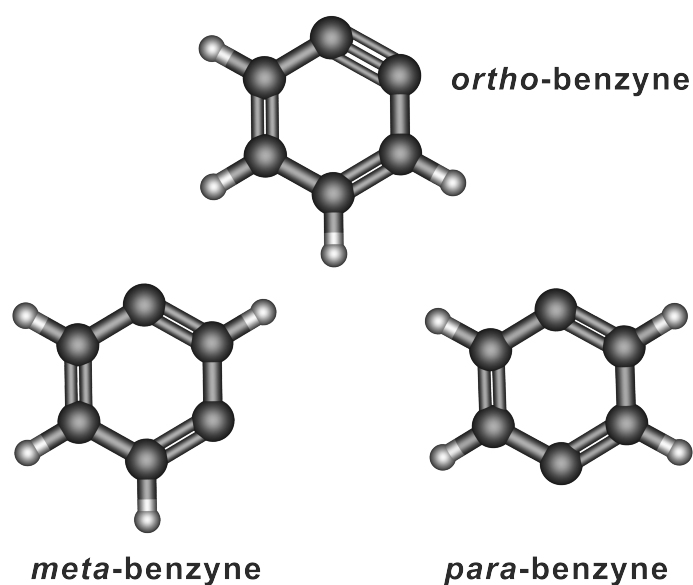


Fig. 1. Scheme of the ortho, para, and meta isomers of benzyne.

8 MHz. The two different frequency throws allow unambiguously negative features produced in the folding of the frequency switching data to be identified. These data allowed the detection of the acetyl cation, CH₃CO⁺ (Cernicharo et al. 2021d), HC₃S⁺ (Cernicharo et al. 2021e), the isomers of C₄H₃N (Marcelino et al. 2021), *l*-H₂C₅ (Cabezas et al. 2021a), vinyl and allenyl acetylene (Cernicharo et al. 2021a,b), ethynyl cyclopropenylidene, cyclopentadiene, and indene (Cernicharo et al. 2021c). Several sulphur-bearing species (NCS, HCCS, H₂CCS, H₂CCCS, C₄S, HCSCN, and HCSCCH) have also been detected with these data (Cernicharo et al. 2021f,g). In addition, some molecules typical of hot cores and corinos (C₂H₃CHO, C₂H₃OH, HCOOCH₃, CH₃OCH₃, CH₃CH₂CN) and species typical of circumstellar envelopes (C₅S, HCCN, HC₄N) were also detected (Agúndez et al. 2021b; Cernicharo et al. 2021a). Last but not least, a significant number of singly and doubly deuterated species, such as HDCCN (Cabezas et al. 2021b), CH₂DC₃N (Cabezas et al. 2021c), and the D and ¹³C doubly substituted isotopologues of HC₃N (Tercero et al., in prep.), have also been observed for the first time in space thanks to QUIJOTE.

The total observing time on the source by May 2021 was 240 h. QUIJOTE is a living line survey, and we expect a total observing time on the source of 450 hours by the end of 2021. The final goal of QUIJOTE, a sensitivity of 0.1 mK (lines of 0.5 mK detected at the 5 σ level), will require around 1000 hours of observing time and will be reached by the winter of 2023–2024.

The sensitivity of our TMC-1 data is better than that of previously published line surveys of this source at the same frequencies (Kaifu et al. 2004) by a factor 20–30. Below 40 GHz the sensitivity is 0.2 mK, increasing slowly up to 0.5 mK at 49.5 GHz. Thanks to this achievement, it has been possible to detect many individual lines from molecules (Cernicharo et al. 2021a) that have been reported only by stacking techniques (Burkhardt et al. 2021). The level of sensitivity we have reached transforms TMC-1 into a source in which, although still far from the spectral confusion limit, the density of lines below 1 mK in intensity is particularly high. TMC-1 can no longer be considered as a line-poor source. Hence, the identification of new species requires a systematic exploration of the rotational transitions of single and double isotopologues of abundant species

² <https://nanocosmos.iff.csic.es/>

³ <http://www.iram.fr/IRAMFR/GILDAS>

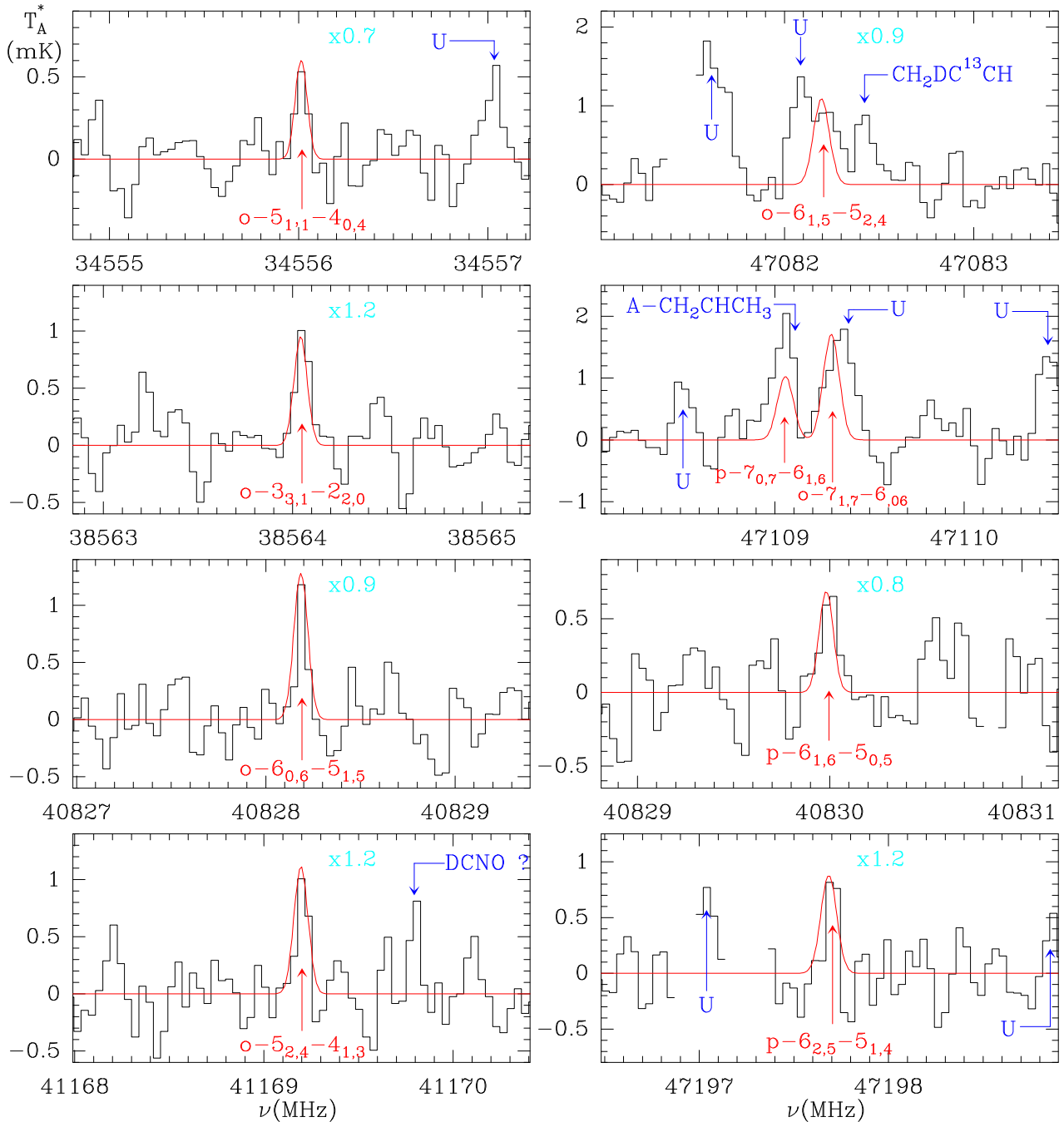


Fig. 2. Subset of the observed lines of o -C₆H₄ in the 31–50 GHz frequency range towards TMC-1 (see Table A.1 for the complete list of detected benzyne lines). The abscissa corresponds to the rest frequency assuming a local standard of rest velocity of 5.83 km s⁻¹. The ordinate is the antenna temperature corrected for atmospheric and telescope losses, in mK. The red line shows the synthetic spectrum obtained from a fit to the observed line profiles, which provides $T_r = 7 \pm 1$ K and $N(o\text{-C}_6\text{H}_4) = (5.0 \pm 1.0) \times 10^{11}$ cm⁻². The rotational quantum numbers are indicated in each panel. Blanked channels correspond to negative features produced in the folding of the frequency switching data. Cyan numbers indicate the multiplicative factor applied to the best model, when needed, to match the observations.

(see e.g. Cabezas et al. 2021b,c; Tercero et al., in prep.) before the detection of a new species can be claimed. In this context, line identification in this work was done using the catalogues MADEX (Cernicharo 2012), CDMS (Müller et al. 2005), JPL (Pickett et al. 1998), and Splatalogue⁴. By May 2021, the MADEX code contained 6369 spectral entries corresponding to the ground and vibrationally excited states, together with the corresponding isotopologues, of 1691 molecules.

3. Results

Our recent discovery of pure hydrocarbon cycles such as cyclopentadiene and indene (Cernicharo et al. 2021c) prompted us to search for other chemically related hydrocarbon cycles, benzyne (o -C₆H₄) being an obvious search candidate. The benzyne molecule is an asymmetric top with a b dipole directed along the C_{2v} symmetry axis, estimated from ab initio calculations to be 1.38 D (Kraka & Cremer 1993). Laboratory data for this species have been taken from Brown et al. (1986), Kukolich et al. (2003), and Robertson et al. 2003. The rotational

⁴ <https://splatalogue.online/advanced1.php>

levels of benzyne are subjected to spin statistics due to the presence of two pairs of equivalent hydrogen nuclei. As shown in Bunker & Jensen (1998), the nuclear statistical weight for the rotational levels with $K_a + K_c$ even and odd is five and three, respectively (ortho and para species; these names refer to the symmetry states and are unrelated to the same names used to distinguish the different isomers). The first para level, $1_{0,1}$, is 0.42 K above the ground ortho state, 0_{00} . Ortho-benzyne was previously searched for towards CRL618 without success (Widicus Wwaver et al. 2007).

An examination of the QUIJOTE data quickly indicates that all ortho lines are detected with antenna temperatures between 0.5 and 1.8 mK. A total of seven ortho lines and four para lines are detected. Figure 2 shows the nine lines detected above 3σ . Two of the lines of para benzyne are detected only at the 3σ level and are not shown in this figure (see Table A.1). Nevertheless, their intensities are compatible with our model predictions. Table A.1 provides the line parameters of the observed lines. One of the para lines, the $3_{3,0}-2_{2,1}$, is fully blended with a line of 2 mK arising from $D^{13}CCCN$ (Tercero et al., in prep.). Three additional lines of the para species are below the 3σ detection limit at the corresponding frequencies (see Table A.1). Some interfering features produce partial blends with three lines of benzyne, as shown in Fig. 2. One of these features arises from a rotational transition of the A species of propylene and overlaps in frequency with the $7_{0,7}-6_{1,6}$ transition of benzyne. From the derived column density of propylene by Marcelino et al. (2007), the expected contribution from the transition of benzyne is 0.5 mK. A couple of unidentified lines also have some partial blend with the $7_{0,7}-6_{1,6}$ and $6_{1,5}-5_{2,4}$ transitions of benzyne. However, the line parameters for these transitions can be derived reasonably well. All remaining lines in the Q band of benzyne are well below our present detection limit. At the present level of sensitivity of QUIJOTE, the number of unidentified lines becomes a concern when any stacking technique is used to detect molecules that produce weak emission. Our detection of benzyne based on the observation of several ortho and para lines is robust, reliable, and provides an accurate estimation of its column density.

An analysis of the observed intensities using a line profile fitting method (Cernicharo et al. 2021e) provides a rotational temperature of 7 ± 1 K and a total (ortho plus para) column density for benzyne of $(5.0 \pm 1.0) \times 10^{11} \text{ cm}^{-2}$. In the fitting procedure we considered the ortho and para levels as those of a single molecule with the corresponding statistical weights (5/3). A separate fit considering the two symmetry species separately and fixing the rotational temperature to 7 K provides similar results and an ortho/para ratio of 1.4 ± 0.6 , which is consistent with the expected value of 5/3.

Adopting an H_2 column density of 10^{22} cm^{-2} for TMC-1 (Cernicharo & Guélin 1987), the abundance of $o\text{-C}_6\text{H}_4$ relative to H_2 is $(5.0 \pm 1) \times 10^{-11}$. This is significantly below those of other cycles, such as $c\text{-C}_3\text{H}_2$, $c\text{-C}_5\text{H}_6$, and $c\text{-C}_9\text{H}_8$ (Cernicharo et al. 2021a).

4. Chemistry

The detection of $o\text{-C}_6\text{H}_4$ in TMC-1 raises interesting questions about its formation. The possible reactions leading to this molecule are discussed in Appendix B. To investigate the overall contribution of reactions (1) and (7) to the formation of $o\text{-C}_6\text{H}_4$ in TMC-1, astrochemical models were exploited (see Fig. 3 and Appendix B). We built a pseudo-time-dependent gas-phase chemical model. We adopted typical parameters of

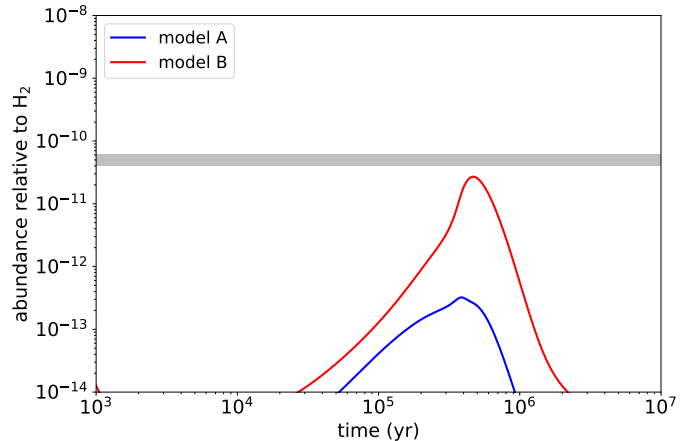


Fig. 3. Calculated fractional abundance of $o\text{-C}_6\text{H}_4$ as a function of time in models A and B (see text). The horizontal grey band corresponds to the observed abundance in TMC-1.

cold dense clouds, namely a gas kinetic temperature of 10 K, a volume density of H_2 of $2 \times 10^4 \text{ cm}^{-3}$, a cosmic-ray ionisation rate of H_2 of $1.3 \times 10^{-17} \text{ s}^{-1}$, a visual extinction of 30 mag, and the set of so-called ‘low-metal’ elemental abundances (see e.g. Agúndez & Wakelam 2013). We note that the volume density of H_2 in TMC-1 could be somewhat higher than that in our adopted value. The main effect of a slight increase in the density is that the abundance curves shift to shorter times, while peak abundances may increase or decrease slightly. The gas-phase chemical network is based on the RATE12 network from the UMIST database (McElroy et al. 2013), with updates relevant for the chemistry of CH_2CCH , CH_2CHCCH , $H_2CCCHCCH$, and $c\text{-C}_5\text{H}_6$ (Agúndez et al. 2021a; Cernicharo et al. 2021a,b,c). Benzyne was included and assumed to be formed by reactions (1) and (7) and destroyed by reactions with C atoms and C^+ and H^+ ions. The peak fractional abundance of $o\text{-C}_6\text{H}_4$ is 3×10^{-13} relative to H_2 (see model A in Fig. 3), which is well below the observed value, $(5 \pm 1) \times 10^{-11}$. This suggests that alternative reactions besides (1) and (7) may contribute to $o\text{-C}_6\text{H}_4$.

Among these reactions, (2), (4), (5), (8), (9), (11), and (12) are unlikely to form $o\text{-C}_6\text{H}_4$ (Appendix B). Reactions (3) and (6) are difficult to implement since the radicals C_5H_3 and C_4H_5 are not included in the UMIST database. Adding ill-defined radical reactions would add more uncertainty to the output of the models. However, the remaining reactions, (13) and (14) and potentially (10), are plausible routes to $o\text{-C}_6\text{H}_4$. Moreover, these reactions involve reactants that are abundant in TMC-1 (Fossé et al. 2001; Cabezas et al. 2021b; Agúndez et al. 2021a). Including these three reactions results in a peak abundance for $o\text{-C}_6\text{H}_4$ of 3×10^{-11} relative to H_2 (model B in Fig. 3), which is in good agreement with the observed value, $(5 \pm 1) \times 10^{-11}$. Therefore, reactions (13), (14), and (10) deserve to be studied experimentally and theoretically in the future to understand how this highly reactive cyclic and aromatic molecule, $o\text{-C}_6\text{H}_4$, can be formed in TMC-1. It should be noted that benzyne could also be formed through ionic routes. For example, the dissociative recombination of the $c\text{-C}_6\text{H}_5^+$ ion with electrons could produce $o\text{-C}_6\text{H}_4$. The precursor ion, $c\text{-C}_6\text{H}_5^+$, could in turn be formed through different ion-neutral reactions, such as $C_4H_3^+ + C_2H_2$ (Anicich 1993; see also Woods et al. 2002) or $C_3H_3^+ + CH_2CCH$.

It would be interesting to investigate whether $o\text{-C}_6\text{H}_4$ could be formed upon the dissociative recombination of $C_6H_5^+$ or C_6 ions with more than five H atoms.

5. Discussion and conclusions

The high abundance of hydrocarbon chains and cycles in TMC-1 suggests that one of the main sites of production of the seeds for PAH formation could be cold dark clouds and that this process could be a transitory one. Figure 3 shows that the peak of formation of *o*-C₆H₄ and other hydrocarbons is produced in a few 10⁵ years. When the density increases due to the collapse of the cloud, most of these large hydrocarbons will stick onto dust grains. The chemistry of ices of cyclopentadiene, benzene, indene, and other species is poorly known as most experiments have been done with large PAHs. The dust grains enriched in these molecules, together with their pristine carbon composition produced during their early formation, will evolve with time and will become the constituents of the solid blocks that produce asteroids and planetesimals during the first stages of star and planet formation. Eventually, some of these grains will be exposed to UV radiation from external and/or internal sources producing photodissociation regions. A significant fraction of the PAH emission observed in these regions could be due to PAHs formed from hydrocarbon-rich ices (Abplanalp et al. 2018; Kaiser & Roessler 1997), and ices of cyclopentadiene, benzene, and indene deposited in a transitory phase of between 10⁵ and 10⁶ yr during the evolution of the cloud (we note that chemical times depend on the volume density and adopted initial physical and chemical conditions). None of these species have been found in the deep *Q*-band line survey of IRC +10216 performed with the Yebes 40 m radio telescope (Pardo et al. 2021). While in the external layers of this carbon-rich circumstellar envelope the abundance of radicals is very high (Agúndez et al. 2017), the chemical time corresponding to these regions is relatively short, ~10⁴ yr, implying that the first cycles may not have had enough time to be formed. A different context is that of carbon-rich protoplanetary nebulae such as CRL 618, where photodissociation and ionisation is enhanced with respect to the AGB phase and where benzene has been found from infrared observations with the Infrared Space Observatory (Cernicharo et al. 2001). Further, distinct temperature ranges from 10 K to a few thousand K facilitate diverse low- and high-temperature molecular mass growth processes (Cernicharo 2004; Kaiser & Hansen 2021).

To summarise, we report in this work the detection of the ortho isomer of benzyne, *o*-C₆H₄, in TMC-1. The observed abundance, $(5 \pm 1) \times 10^{-11}$ relative to H₂, can be nicely reproduced with fractional abundances of 3×10^{-11} considering that *o*-C₆H₄ is formed by the neutral-neutral reactions C₂H + CH₂CHCCH and C + C₅H₅ and possibly through the reactions C₄H + C₂H₄, C₃H + CH₂CCH₂, and C₃H₂ + C₃H₃. With a sensitive line survey such as QUIJOTE, the discovery of new molecules can be performed in the classical line by line detection method. Hence, QUIJOTE provides unambiguous detection of new molecular species and reliable column density determinations.

Acknowledgements. We thank ERC for funding through grant ERC-2013-SyG-610256-NANOCOSMOS. M.A. thanks MICIU for grant RyC-2014-16277. We also thank Ministerio de Ciencia e Innovación of Spain (MICIU) for funding support through projects AYA2016-75066-C2-1-P, PID2019-106110GB-I00, PID2019-107115GB-C21/AEI/10.13039/501100011033, and PID2019-10623 5GB-I00.

References

Abplanalp, M. J., Jones, B. M., & Kaiser, R. I. 2018, *Phys. Chem. Chem. Phys.*, **20**, 5435
 Agúndez, M., & Wakelam, V. 2013, *Chem. Rev.*, **113**, 8710

Agúndez, M., Cernicharo, J., Quintana-Lacaci, G., et al. 2017, *A&A*, **601**, A4
 Agúndez, M., Cabezas, C., Tercero, B., et al. 2021a, *A&A*, **647**, L10
 Agúndez, M., Marcelino, N., Tercero, B., et al. 2021b, *A&A*, **649**, L4
 Anicich, V. G. 1993, *J. Phys. Chem. Ref. Data*, **22**, 1469
 Bunker, P. R., & Jensen, P. 1998, *Molecular Symmetry and Spectroscopy*, 2nd edn. (Ottawa: NRC Research Press)
 Burkhardt, A. M., Lee, L. K., Bryan Changala, P., et al. 2021, *ApJ*, **913**, L18
 Brown, R. D., Godfrey, P. D., & Rodler, M. 1986, *J. Am. Chem. Soc.*, **108**, 1296
 Cabezas, C., Tercero, B., Agúndez, M., et al. 2021a, *A&A*, **650**, L9
 Cabezas, C., Endo, Y., Roueff, E., et al. 2021b, *A&A*, **646**, L1
 Cabezas, C., Roueff, E., Tercero, B., et al. 2021c, *A&A*, **650**, L15
 Canosa, A., Sims, I. R., Travers, D., et al. 1997, *A&A*, **323**, 644
 Cernicharo, J. 1985, *Internal IRAM Report* (Granada: IRAM)
 Cernicharo, J. 2004, *ApJ*, **608**, L41
 Cernicharo, J. 2012, *EAS Publ. Ser.*, **251**
 Cernicharo, J., & Guélin, M. 1987, *A&A*, **176**, 299
 Cernicharo, J., Heras, A. M., Tielens, A. G. G. M., et al. 2001, *ApJ*, **546**, L123
 Cernicharo, J., Marcelino, N., Pardo, J. R., et al. 2020a, *A&A*, **641**, L9
 Cernicharo, J., Marcelino, N., Agúndez, M., et al. 2020b, *A&A*, **642**, L8
 Cernicharo, J., Marcelino, N., Agúndez, M., et al. 2020c, *A&A*, **642**, L17
 Cernicharo, J., Agúndez, M., Cabezas, C., et al. 2021a, *A&A*, **647**, L2
 Cernicharo, J., Cabezas, C., Agúndez, M., et al. 2021b, *A&A*, **647**, L3
 Cernicharo, J., Agúndez, M., Cabezas, C., et al. 2021c, *A&A*, **649**, L15
 Cernicharo, J., Cabezas, C., Baillieux, S., et al. 2021d, *A&A*, **646**, L7
 Cernicharo, J., Cabezas, C., Endo, Y., et al. 2021e, *A&A*, **646**, L3
 Cernicharo, J., Cabezas, C., Agúndez, M., et al. 2021f, *A&A*, **648**, L3
 Cernicharo, J., Cabezas, C., Agúndez, M., et al. 2021g, *A&A*, **650**, L14
 Chastaing, D., James, P. L., Sims, I. R., & Smith, I. W. M. 1998, *Faraday Discuss.*, **109**, 165
 Cherchneff, I., Barker, J. R., & Tielens, A. G. G. M. 1992, *ApJ*, **401**, 269
 Doddipatla, S., Galimova, G. R., Wei, H., et al. 2021, *Sci. Adv.*, **7**, eabd4044
 Fossé, D., Cernicharo, J., Gerin, M., & Cox, P. 2001, *ApJ*, **552**, 168
 Hahndorf, I., Lee, Y. T., & Mebel, A. M. 2000, *J. Chem. Phys.*, **113**, 9622
 Hahndorf, I., Lee, Y. T., Kaiser, R. I., et al. 2002, *J. Chem. Phys.*, **116**, 3248
 Hirsch, F., Reusch, E., Constantinidis, P., et al. 2018, *J. Phys. Chem. A*, **122**, 9563
 Joblin, C., & Cernicharo, J. 2018, *Science*, **359**, 156
 Jones, B. M., Zhang, F., Kaiser, R. I., et al. 2011, *Proc. Natl. Acad. Sci. USA*, **108**, 452
 Kaifu, N., Ohishi, M., Kawaguchi, K., et al. 2004, *PASJ*, **56**, 69
 Kaiser, R. I. 2002, *Chem. Rev.*, **102**, 1309
 Kaiser, R. I., & Hansen, N. 2021, *J. Phys. Chem. A*, **125**, 3826
 Kaiser, R. I., & Roessler, K. 1997, *ApJ*, **475**, 144
 Kraka, E., & Cremer, D. 1993, *Chem. Phys. Lett.*, **216**, 333
 Kukolich, S. G., Tanjaroon, C., McCarthy, M. C., & Thaddeus, P. 2003, *J. Chem. Phys.*, **119**, 4353
 Marcelino, N., Cernicharo, J., & Agúndez, M. 2007, *ApJ*, **665**, L127
 Marcelino, N., Agúndez, M., Tercero, B., et al. 2020, *A&A*, **643**, L6
 Marcelino, N., Tercero, B., Agúndez, M., & Cernicharo, J. 2021, *A&A*, **646**, L9
 Martínez, L., Santoro, G., Merino, P., et al. 2020, *Nat. Astron.*, **4**, 97
 McCabe, M. N., Hemberger, P., Reusch, E., et al. 2020, *J. Phys. Chem. Lett.*, **11**, 2859
 McElroy, D., Walsh, C., Markwick, A. J., et al. 2013, *A&A*, **550**, A36
 McGuire, B. A., Burkhardt, A. M., Kalenskii, S., et al. 2018, *Science*, **359**, 202
 McGuire, B. A., Loomis, R. A., Burkhardt, A. M., et al. 2021, *Science*, **371**, 1265
 Mebel, A. M., & Kaiser, R. I. 2015, *Int. Rev. Phys. Chem.*, **17**, 21564
 Müller, H. S. P., Schlöder, F., Stutzki, J., & Winnewisser, G. 2005, *J. Mol. Struct.*, **742**, 215
 Olsen, J. F. 1971, *J. Mol. Struct.*, **8**, 307
 Pardo, J. R., Cernicharo, J., & Serabyn, E. 2001, *IEEE Trans. Antennas Propag.*, **49**, 12
 Pardo, J. R., Cernicharo, J., Tercero, B., et al. 2021, *A&A*, submitted
 Parker, D. S. N., Zhang, F., Kim, Y. S., et al. 2012, *Proc. Natl. Acad. Sci. USA*, **109**, 53
 Pickett, H. M., Poynter, R. L., Cohen, E. A., et al. 1998, *J. Quant. Spectrosc. Radiat. Transf.*, **60**, 883
 Pilleri, P., Joblin, C., Boulanger, F., & Onaka, T. 2015, *A&A*, **577**, A16
 Robertson, E. G., Godfrey, P. D., & McNaughton, D. 2003, *J. Mol. Spectrosc.*, **217**, 123
 Tercero, F., López-Pérez, J. A., Gallego, J. D., et al. 2021, *A&A*, **645**, A37
 Widicus Wwaver, S., Remijan, A. J., McMahon, R. J., & McCall, B. J. 2007, *ApJ*, **671**, L153
 Woods, P. M., Millar, T. J., & Zijlstra, A. A. 2002, *ApJ*, **574**, L167
 Zhang, F., Parker, D., Kim, Y. S., et al. 2011, *ApJ*, **728**, 141

Appendix A: Benzynes line parameters

Line parameters were derived from a Gaussian fit to the observed lines using the GILDAS package. A velocity coverage of $\pm 15 \text{ km s}^{-1}$ was selected for each line. Observed frequencies were derived assuming a local standard of rest velocity of 5.83 km s^{-1} (Cernicharo et al. 2020b). Observed velocities for the detected lines were determined assuming that rest frequencies are those predicted from the rotational and distortion constants provided by the fit to the laboratory data (Brown et al.

1986; Kukolich et al. 2003; Robertson et al. 2003). The predicted frequencies in MADEX (Cernicharo 2012) agree within 1-5 kHz with those of the CDMS (Müller et al. 2005). Differences between predicted and observed frequencies never exceed $1.5\sigma\Delta\nu$, where $\Delta\nu$ is the estimated frequency uncertainty of the observed lines. The averaged V_{LSR} from the 11 observed lines of benzyne is $5.80\pm 0.05 \text{ km s}^{-1}$, a value similar to that derived from all lines of HC_5N and its isotopologues in the Q band (Cernicharo et al. 2020b).

Table A.1. Observed line parameters of benzyne.

Transition	ν_{pred}^a (MHz)	ν_{obs}^b (MHz)	$\int T_A^* dv^c$ (mK km s ⁻¹)	ν_{LSR}^d (km s ⁻¹)	$\Delta\nu^e$ (km s ⁻¹)	T_A^{*f} (mK)	N
ortho state							
4 _{1,3} – 3 _{2,2}	33482.756(1)	33482.786(30)	0.34(07)	5.56(07)	0.66(18)	0.48(17)	
5 _{1,5} – 4 _{0,4}	34556.013(2)	35556.013(30)	0.36(10)	5.83(09)	0.63(18)	0.55(18)	
3 _{3,1} – 2 _{2,0}	38564.042(1)	38564.054(30)	0.74(15)	5.74(07)	0.68(17)	1.02(20)	
6 _{0,6} – 5 _{1,5}	40828.169(4)	40828.169(20)	0.54(11)	5.83(05)	0.45(10)	1.19(22)	
5 _{2,4} – 4 _{1,3}	41169.208(2)	41169.205(20)	0.56(13)	5.85(07)	0.48(12)	1.09(24)	
6 _{1,5} – 5 _{2,4}	47082.207(4)	47082.207(30)	0.87(30)	5.83(16)	0.87(30)	0.94(27)	
7 _{1,7} – 6 _{0,6}	47109.298(7)	47109.345(30)	1.91(25)	5.53(10)	1.02(15)	1.77(35)	A
para state							
5 _{0,5} – 4 _{1,4}	34543.093(2)					≤0.70	
4 _{2,3} – 3 _{1,2}	35656.830(1)					≤0.75	
5 _{1,4} – 4 _{2,3}	40595.926(2)	40595.919(30)	0.16(08)	5.90(12)	0.40(15)	0.47(17)	
6 _{1,6} – 5 _{0,5}	40829.994(4)	40830.000(30)	0.55(19)	5.79(13)	0.78(39)	0.67(27)	
3 _{3,0} – 2 _{2,1}	41071.944(1)						B
4 _{3,2} – 3 _{2,1}	45028.539(1)					≤0.75	
7 _{0,7} – 6 _{1,6}	47109.056(7)	47109.044(20)	1.63(21)	5.90(08)	0.80(13)	1.92(27)	C
6 _{2,5} – 5 _{1,4}	47197.685(4)	47197.708(30)	0.45(11)	5.72(20)	0.45(15)	0.95(26)	

Notes. Values between parentheses correspond to the uncertainties of the parameters in units of the last significant digits. Upper limits correspond to 3σ values. ^(a)Predicted frequency from the rotational and distortion constants derived from a fit to the lines observed by Brown et al. (1986), Kukolich et al. (2003), and Robertson et al. (2003). ^(b)Observed frequency assuming a ν_{LSR} of 5.83 km s^{-1} . ^(c)Integrated line intensity in mK km s⁻¹. ^(d) ν_{LSR} assuming that the predicted frequencies are the rest frequencies of the lines (in km s⁻¹). ^(e)Line width at half intensity derived by fitting a Gaussian function to the observed line profile (in km s⁻¹). ^(f)Antenna temperature in millikelvin. ^(A)Possibly a blend with a U line at +35 kHz of the predicted frequency. ^(B)Blended with a line of D¹³CCCN. Fit unreliable. ^(C)Blended with a line of CH₂CHCH₃ with an expected intensity of 0.5 mK.

Appendix B: The chemical network for the formation of benzyne

The low number densities of the reactants along with the typical 10 K translational temperature of a cold starless core such as TMC-1 only support barrierless and exoergic bimolecular reactions. Focusing on neutral-neutral reactions, the scheme is $A + B \rightarrow [AB]^* \rightarrow C + D$, where A and B represent the reactants, $[AB]^*$ is the reaction intermediate(s), and C and D are the products (Kaiser 2002). In TMC-1, the newly detected *o*-C₆H₄ defines the product C; atomic hydrogen represents one of the most prominent counter fragments, D, that carry away a significant amount of the total angular momentum. This concludes that $[AB]^*$ has to fulfil the stoichiometry of $[C_6H_5]^*$. Since the intermediate holds six carbon atoms, this can be achieved in bimolecular reactions in C₁-C₅, C₂-C₄, and C₃-C₃ systems with reactants at various degrees of hydrogenation. In principle, the following reactions, (1) to (14), could yield rovibrationally excited $[C_6H_5]^*$ reaction intermediates, which undergo unimolecular decomposition via atomic hydrogen loss to form the newly detected *o*-C₆H₄ molecule.

- (1) $C + C_5H_5 \rightarrow o\text{-}C_6H_4 + H$
- (2) $CH + C_5H_4 \rightarrow o\text{-}C_6H_4 + H$
- (3) $CH_2 + C_5H_3 \rightarrow o\text{-}C_6H_4 + H$
- (4) $CH_3 + C_5H_2 \rightarrow o\text{-}C_6H_4 + H$
- (5) $CH_4 + C_5H \rightarrow o\text{-}C_6H_4 + H$
- (6) $C_2 + C_4H_5 \rightarrow o\text{-}C_6H_4 + H$
- (7) $C_2H + C_4H_4 \rightarrow o\text{-}C_6H_4 + H$
- (8) $C_2H_2 + C_4H_3 \rightarrow o\text{-}C_6H_4 + H$
- (9) $C_2H_3 + C_4H_2 \rightarrow o\text{-}C_6H_4 + H$
- (10) $C_2H_4 + C_4H \rightarrow o\text{-}C_6H_4 + H$
- (11) $C_2H_5 + C_4 \rightarrow o\text{-}C_6H_4 + H$
- (12) $C_3 + C_3H_5 \rightarrow o\text{-}C_6H_4 + H$
- (13) $C_3H + C_3H_4 \rightarrow o\text{-}C_6H_4 + H$
- (14) $C_3H_2 + C_3H_3 \rightarrow o\text{-}C_6H_4 + H$.

Among these reactions, only the reaction between the ethynyl radical (C₂H) and vinylacetylene (CH₂CHCCH), reaction (7), has been studied via crossed molecular beam experiments and electronic structure calculations (Zhang et al. 2011). This reaction is barrierless and exoergic, and thus it is expected to be fast at low temperatures. This finding is in line with the known high reactivity of C₂H radicals with unsaturated hydrocarbons at low temperatures (Chastaing et al. 1998), revealing rates of up to $4 \times 10^{-10} \text{ cm}^3 \text{ s}^{-1}$. Moreover, Zhang et al. (2011) predicted that *o*-C₆H₄ is formed with a branching ratio of up to 20% at 10 K, thus providing an effective rate of $8 \times 10^{-11} \text{ cm}^3 \text{ s}^{-1}$. Reaction (7) is thus a plausible route to benzyne in TMC-1. Further, in analogy to the C(³P)-benzene system (Hahndorf et al. 2002), the reaction of atomic carbon (C(³P)) with cyclopropadienyl (*c*-C₅H₅) – although studied neither experimentally nor computationally – is expected to form *o*-C₆H₄ plus atomic hydrogen (reaction (1)). Hahndorf et al. (2000) predicted

computationally that the propargyl radical (C₃H₃) can react barrierlessly and exoergically with the vinyl radical (C₂H₃) on the singlet surface to form *c*-C₅H₅ plus atomic hydrogen, thus providing the *c*-C₅H₅ required for reaction (1).

B.1. Discounted reactions to benzyne

Reaction (2) has never been studied in the laboratory with any isomer such as methyldiacetylene (HCCCCCH₃), penta-1,4-diyne (CH₂(C₂H)₂), or 1,2,3,4-pentatetraene (H₂CCCCCH₂). Rate constant measurements of methyldiyne (CH) with unsaturated hydrocarbons by Canosa et al. (1997) reveal barrierless pathways with rates of a few $10^{-10} \text{ cm}^3 \text{ s}^{-1}$. However, crossed molecular beam reactions indicate that the CH radical adds to the double or triple bond of, for example, acetylene, ethylene, diacetylene, allene, and methylacetylene, followed by isomerisation through the ring opening and/or hydrogen shifts, followed by hydrogen atom losses. Six-membered ring formation only occurs through the ring expansion of an existing five-membered ring (i.e. a hypothetical cyclic *c*-C₅H₄ isomer). However, no confirmed formation routes to cyclic *c*-C₅H₄ are known so far; therefore, we do not include reaction (2) as a contributor to benzyne.

Reaction (4), which has never been studied either computationally nor experimentally, involves the addition of a methyl radical (CH₃) to a triplet carbene (HCCCCCH). The addition of a methyl radical to triple bonds of the ethynyl moiety involves barriers of up to 50 kJ mol⁻¹, which cannot be overcome in TMC-1. Methyl radicals could add barrierlessly to the central carbon atom, which essentially carries the unpaired electrons. However, this requires small, nearly zero-impact parameters and an extensive reorganisation of the carbon skeleton; therefore, although exoergic by 207 kJ mol⁻¹ overall, the formation of benzyne is unlikely.

Reaction (5) represents a direct reaction that leads, via hydrogen abstraction, to a methyl radical plus C₅H₂ molecules; although never studied experimentally, this hydrogen abstraction is expected to have a barrier. Further, this reaction is endoergic by 27 kJ mol⁻¹ and hence cannot take place at 10 K. Reaction (5) cannot form *o*-C₆H₄ + H at 10 K since hydrogen abstraction represents the only feasible pathway.

Reaction (8) has an entrance barrier of addition of the C₄H₃ with its radical centre to the carbon-carbon triple bond of acetylene 25–37 kJ mol⁻¹. Hence, its reaction is closed at 10 K as well.

Reaction (9) involves the reaction of a vinyl radical with diacetylene; reactions of vinyl radicals with closed-shell olefins and alkynes have entrance barriers of 10 to 35 kJ mol⁻¹, which cannot be overcome in TMC-1. This has been confirmed computationally (Zhang et al. 2011). Finally, reaction (11) and, in particular, reaction (12) likely have entrance barriers (Mebel & Kaiser 2015).